Anodization of Aluminum in Highly Viscous Phosphoric Acid. PART 2: Investigation of Anodic Oxide Formation and Dissolution Rates

Lissy Berndt[1,2], Malte Kleemeier[1], Karsten Thiel[1], Malte Burchardt[1], Andreas Hartwig[1,2,]*

[1] Fraunhofer Institute for Manufacturing Technology and Advanced Materials IFAM, Wiener Straße 12, D-28359 Bremen, Germany
[2] University of Bremen, Department 2 Biology/Chemistry, Leobener Str. 2, D-28359 Bremen, Germany
[*]E-mail: Andreas.hartwig@ifam.fraunhofer.de

A novel self-sticking adhesive tape for the local anodization of aluminum that can be removed without residue after anodization was developed. The extremely high viscosity of the electrolyte used in the anodization tape is the main difference to conventional bath anodization in aqueous phosphoric acid. Through the application of a step-like voltage program with abrupt changes in the anodization voltage, sublayers within the porous part of the anodic oxide were formed and then examined using transmission electron microscopy (TEM). The sublayers enable an estimation of the oxide formation and dissolution rates of bath and tape anodization. Both rates depend on the anodization voltage. At the beginning of the anodization process, the oxide formation rates for bath anodization and tape anodization were very similar. At a voltage of 25 V, a formation rate of 0.9 nm s^{-1} was obtained for bath anodization, compared to 0.8 nm s^{-1} for tape anodization. However, the formation rate for the anodization tape slows down considerably in the later stages of anodization. This effect, which was not found for bath anodization, can be attributed to a local aging of the highly viscous electrolyte used for the anodization tape. Another special feature of the anodization tape is a very low rate of chemical oxide dissolution (≤ 0.04 nm s^{-1}). In contrast, dissolution rates in the range of 0.1 to ≥ 0.2 nm s^{-1} were found for bath anodization, which are typical for strongly dissolving electrolytes such as phosphoric acid.

1. INTRODUCTION

Anodization is a widely used electrochemical surface treatment for metals such as aluminum. As a pre-treatment prior to adhesive bonding or paint application, the porous anodic oxide formed by

this process provides excellent adhesion. For anodization, the aluminum part is immersed in an acidic solution and a voltage is applied between the part (anode) and an auxiliary electrode (cathode).

Recently, anodization processes in media with extremely high viscosity have been investigated. These processes form the basis for self-sticking adhesive tapes that can be employed for local anodization [1, 2]. The main component of this anodization tape is a water-based adhesive that contains phosphoric acid as an electrolyte. A steel mesh is inserted as a cathode into the polymer matrix of the adhesive tape. The application, preparation, and composition of the anodization tape have been described in detail in a previous publication [1]. The application of anodization tapes offers some advantages when compared to other local anodization techniques [3-7]. Local anodization is particularly useful for such applications as the rework, repair, maintenance, or partial treatment of large components where conventional bath anodization is not possible.
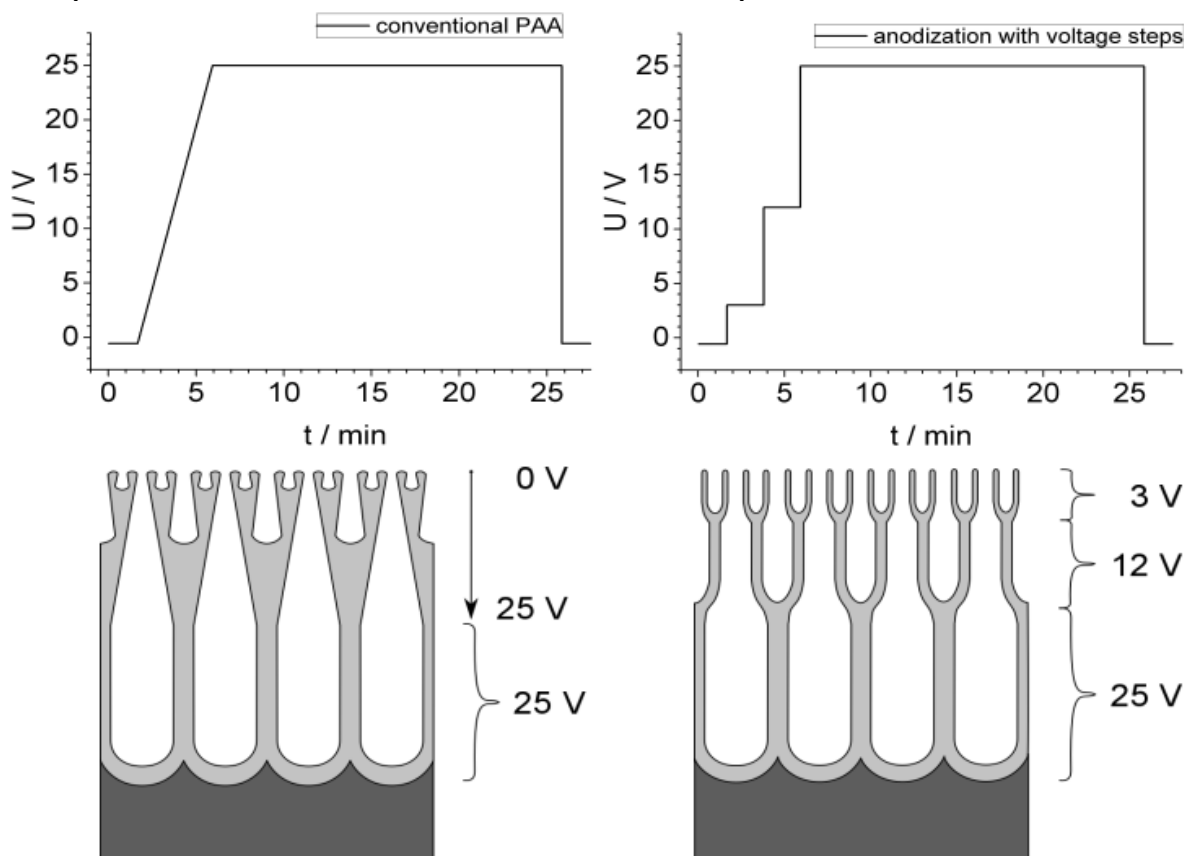
Figure 1. Schematic diagram of the pore structure of the anodic oxide resulting from an anodization process with a continuously ramped up voltage to a constant plateau (left side) and a process where the ramp was replaced by series of discrete voltage steps (right).

For an effective application of the anodization tape, the differences to conventional bath anodization need to be known. Due to the highly viscous electrolyte of the anodization tape, it can be expected that the oxide formation and oxide dissolution are slowed down, but the exact mechanism remains unclear.

The special features of the anodic oxide formed by employing the anodization tape have already been investigated in previous papers and have also been compared to the properties of anodic

oxide resulting from conventional anodization in a bath [1, 2]. The most recent paper [2] was focused on the compact barrier oxide in direct vicinity to the aluminum substrate. Its electrical parameters, such as barrier resistance and capacity, were measured using an *in-situ* electrochemical impedance spectroscopy (*in-situ* EIS) technique. This required the anodization to be carried out under stationary conditions. The usual ramping up of the voltage during the anodization process was therefore replaced by a series of discrete voltage steps (see Fig. 1).

As the pore size in porous oxides depends on the anodization voltage, each voltage step results in a sublayer with a distinct pore diameter. This offers the opportunity to compare the two anodization processes (in the following termed as "bath anodization" and "tape anodization") with regard to a) the formation rate of the anodic oxide due to the electrochemical oxidation of aluminum and b) the rate of dissolution of the oxide by the chemical attack of the electrolyte (phosphoric acid). In this paper we investigate in detail how oxide formation and dissolution are influenced by the exceptionally high viscosity of the electrolyte used for the anodization tape. To this end, the structures of the porous part of the anodic oxide that were formed at each voltage step and exposed to the electrolyte for different times were evaluated on the basis of TEM images.

2. EXPERIMENTAL

2.1 Aluminum specimens and electrolytes

For bath and tape anodization, specimens of commercially pure aluminum AA1050A were used; their nominal composition according to EN 573-3 is given in Table 1.

Table 1. Nominal composition of aluminum AA1050A (wt.%), according to EN 573-3

	Al	Fe	Si	Ti	Mn	Mg	Zn	Cu
AA1050	99.5	0.26	0.08	0.021	0.005	0.004	0.002	0.002

For the tape anodization, a multi-stage cleaning process was used for the aluminum sheets. The stages of cleaning are shown in Table 2. Between all steps, the specimens were spray rinsed with deionized (DI) water for 30 s, immersion rinsed in DI water for 3 min, and spray rinsed again with DI water for 30 s.

Table 2. Multi-stage cleaning of aluminum specimens for tape anodization

Stage of cleaning	Solution composition	Temperature	Time
Degreasing	40 g L^{-1} Turco 4215 NC (Henkel) in water	60 °C	5 min
Etching	40 g L^{-1} Aluminetch No. 2 (Henkel) in water	60 °C	1 min
Pickling	180 mL L^{-1} Turco Liquid Smutgo NC (Henkel) in water	36 °C	10 min
Drying	-	50 °C	30 min

The dried aluminum sheets were stored in an aluminum pouch under an argon atmosphere until the application of the anodization tape.

The specimens for bath anodization were designed for multiple uses. Aluminum discs (1 cm diameter) were embedded in polyetheretherketone or polytetrafluoroethylene holders around 2 cm in diameter. The embedded discs required both mechanical and chemical treatment to eliminate the previous anodization layers. The mechanical pre-treatment of the aluminum specimens is shown in Table 3.

Table 3. Mechanical surface pre-treatment of aluminum specimens for bath anodization

Stage of surface pretreatment	Fabric / paper	Agent
Grinding	Silicon carbide abrasive paper (2500 and 4000 grit)	Water
Polishing	Rugged synthetic fabric MD-Plus (Struers)	Diamond-based suspension with a particle size of 3 μm Cooling medium: ethanol/ethylene glycol
Mechanical finish	Neoprene fabric MD-Chem (Struers)	Polishing agent: silica suspension with particle size of 0.04 μm
Rinsing	-	Water and ethanol

After mechanical surface treatment, the specimens were stored for at least 24 h in a desiccator with silica gel as a drying agent to obtain a reproducible natural oxide layer. Just prior to bath anodization, the specimens were pickled in 180 mL L^{-1} Turco Liquid Smutgo NC (Henkel) for 10 min at 36 °C and then intensively rinsed in DI water for 3 min.

The electrolyte for bath anodization (PAA, phosphoric acid anodization) was 12 wt.% phosphoric acid (Sigma Aldrich) according to ASTM D 3933 - 98 [8].

The components of the adhesive for tape anodization were polyacrylic acid 40 wt.% solution in water (DEGAPAS 4104S, Evonik), polyvinyl alcohol (Mowiol 10-98, Kuraray), fumed silica (Aerosil 200, Evonik), glycerol, lactic acid, and phosphoric acid 85% (the latter three chemicals were obtained from Sigma-Aldrich). Detailed information about the preparation of anodization tapes has been published in a previous publication [1].

2.2. Anodization

A potentiostat GAMRY Reference 3000 with a high voltage regime was used for both bath and tape anodization. The device was controlled by a personal computer using the GAMRY Framework software package 6.20. The electrode arrangement for bath and tape anodization is shown in Fig. 2.
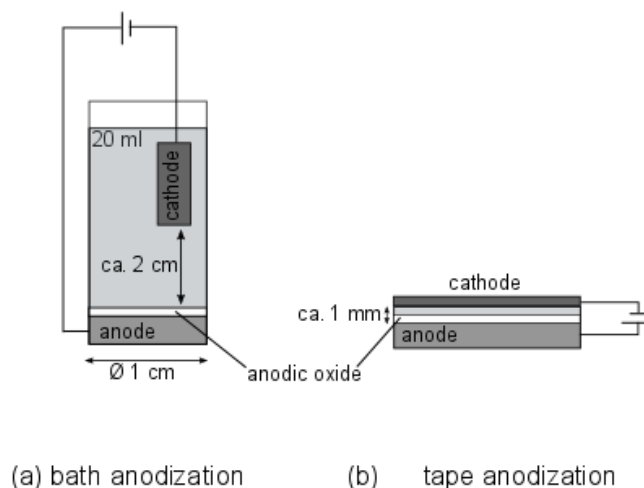
(a) bath anodization   (b)   tape anodization

Figure 2. Schematic diagram of the setup for the anode and cathode when carrying out anodization in a bath (a) and by using the anodization tape (b).

For tape anodization, after the application of the anodization tape to the aluminum surface, the specimen and metal mesh in the tape were connected to the potentiostat in a two-electrode setup (Fig. 2b). The resistance of the electrolytes used in the anodization bath and in the tape adhesive was obtained from electrochemical impedance spectroscopy (*in-situ* EIS) [2]. For the anodization bath, the cross-section normalized electrolyte resistance was 4.0 ± 0.1 Ωcm^2. The corresponding value for anodization tape was 5.0 ± 0.3 Ωcm^2.

Tape anodization was carried out at a temperature of 23 °C. The actual temperature was monitored by attaching a thermocouple to the aluminum substrate. During anodization, only a very moderate ohmic heating could be noted, and the temperature increase never exceeded 6 K. The ohmic heating for bath anodization showed an increase in the same range, namely 5 K from room temperature of 23 °C. After anodization, the tape was removed and the sample was intensively rinsed by immersion in DI water in an ultrasonic bath for 5 min. Before and after the immersion rinsing, the sample was spray rinsed with DI water.

For bath anodization, a top-mounted cell with a volume of 20 ml on the embedded aluminum discs (working electrode) was used (Fig. 2a). A platinum sheet as the counter electrode and a saturated calomel electrode (SCE) as the reference electrode completed the three-electrode setup. For easier reading, the measured potentials in the three-electrode setup were termed as the voltage. The vertical arrangement of the electrodes corresponds to the setup used for the tape anodization. As with the tape anodization, the specimens were intensively rinsed and immersed in DI water in an ultrasonic bath for 5 min after anodization.

Anodization was carried out in the voltage-controlled mode. The sequence of the applied voltages in dependence on the time is shown in Fig. 3; this was the same as in previous investigations of *in-situ* EIS measurement during anodization [2].
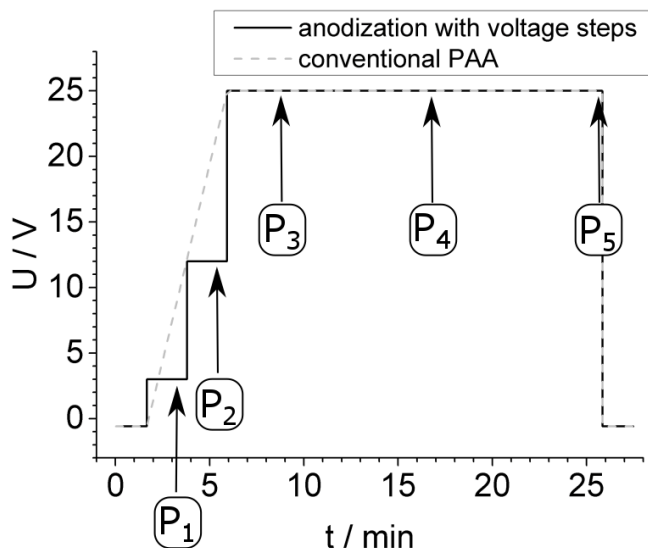
Figure 3. Schematic diagram of the anodization process with steps at 3 V and 12 V. Arrows indicate times of measurement points for TEM and EFTEM sampling.

The sequence of voltage steps corresponds to the conventional bath process with a voltage ramp of 6 V min^{-1} from OCP (open circuit potential) to 25 V and a voltage hold of 20 min [8]. The voltage ramp was replaced by 3 voltage steps from OCP to 3 V, 12 V, and 25 V. The step duration was about 125 s, corresponding to a voltage ramp of 6 V min^{-1}. The black arrows in Fig. 3 indicate the times of the measurement points P_n for the TEM examinations. Slight deviations in treatment times occurred due to different periods of *in-situ* EIS measurements, which were performed in parallel and are published elsewhere [2]. The average times of sampling $t(P_n, U)$ are summarized in Table 4 and were the same for bath and tape anodization.

Table 4. Average times of sampling for TEM and EFTEM measurement

$t(P_n, U)$ / s		Measurement points for bath and tape anodization				
		P_1	P_2	P_3	P_4	P_5
U / V	OCP	107	107	107	107	107
	3	86	131	131	131	131
	12	-	86	141	141	141
	25	-	-	95	634	1165

2.3. Focused ion beam (FIB)

A transmission electron microscope (TEM) was used for the nanostructural analysis of the barrier and porous layers on the anodic oxide. For the examination, thin electron transparent lamellas had to be prepared by focused ion beam (FIB) preparation. A Ga ion beam in a FEI Helios 600 dualbeam machine (Hillsboro, USA) was used. First, Pt/Pd were deposited on the anodic oxide surface in a Cressington Turbo sputter coater 208 (Watford, UK). The thinly deposited layer of a few

nanometers prevented the charging of the sample by the FIB. For the preservation of the anodic oxide during FIB preparation, the surface was protected by a carbon deposition layer. For this, 500 nm carbon was deposited by means of electron beam induced deposition, followed by carbon deposition layers of about 2-3 µm by means of ion beam induced deposition. Subsequently, a relatively thick lamella was cut at a 30 kV ion beam energy, transferred and mounted to an Omniprobe TEM grid. Then the lamella was further thinned to electron transparency and finally polished (at a 5 kV ion beam energy). The final thickness of the TEM lamellas was 50 nm to 100 nm. Due to the fact that the porous oxide layer leads to a pronounced curtaining of the lamella in the preparation process, the lamella was rotated by 180 degrees in the FIB so that the inevitable curtains ran from the porous oxide into the protection layer and not across the barrier layer into the aluminum substrate.

2.4. Transmission electron microscopy (TEM)

For the investigation of the barrier and porous layer thicknesses, TEM was applied using a FEI Tecnai F20 S-TWIN microscope equipped with a GATAN imaging filter (GIF2001).

The microscope was operated at an accelerating voltage of 200 kV with a field-emission gun (FEG), resulting in a point resolution of 2.4 Å. The TEM images were recorded with the slow-scan CCD camera integrated into the GIF (1024x1024 pixel array). No binning was used for the TEM images.

3. RESULTS AND DISCUSSION

3.1 Voltage curve and current density-time response

An important characteristic reflecting the electrochemical reactions during anodization is the current density-time response. For bath and tape anodization, the current density-time responses are shown in Fig. 4.
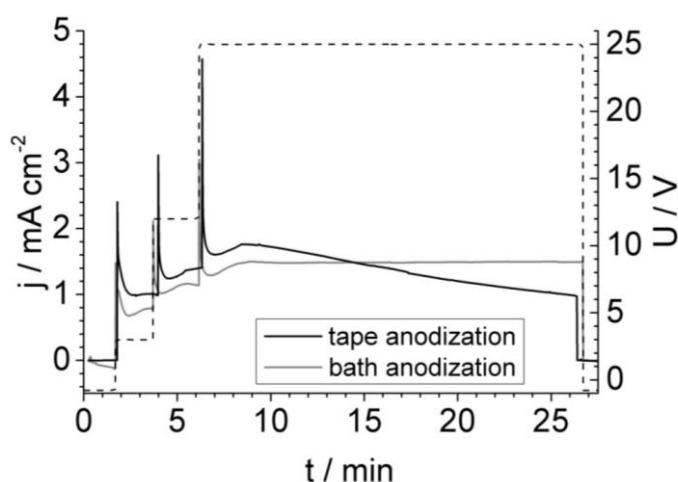

Figure 4. Current density-time responses and voltage curves for tape (black) and bath (light grey) anodization of AA1050A at 23 °C.

The current density is composed of the current densities associated with oxide formation (i.e. thickening of the barrier type oxide layer) and chemical and electric field assisted oxide dissolution, direct injection of aluminum ions into the electrolyte, and charging of the electrochemical double layer [9]. Directly after each voltage step, the charging of the electrochemical double layer and the delayed thickening of the barrier layer led to an abrupt increase in current density. After that, the current density decreased quickly and reached a nearly constant value after passing a small local minimum.

A significant difference in current density between bath and tape anodization is that the current density continuously decreased during the final voltage hold for tape anodization. This is most likely the result of a limitation of mass transport and of a reduction in the effective area available for anodization [2].

3.2. The role of electrolyte resistance and anodization temperature

As shown in Fig. 2, the geometrical setup for bath and tape anodization is quite different, especially regarding the distance between anode and cathode. Therefore, in order to carry out a meaningful analysis of how the growth of anodic oxide is influenced by the viscosity of the electrolyte, it first must be excluded that the differences found for bath and tape anodization originate from factors related to the geometrical setup. Notably, the electrolyte resistance and the temperature during the anodization process may be dependent on geometrical aspects.

For a given externally applied voltage, the ohmic drop in the electrolyte diminishes the potential difference present at the barrier oxide. Since important properties of the anodic oxide, such as the thickness of the compact barrier layer or the pore size of the porous layer, depend on the potential difference, the resistance of the electrolyte may indirectly influence the oxide morphology. It could be expected that the resistance of the electrolyte in the anodization tape is much smaller than in bath anodization, because here the anode and cathode are placed at a close distance of 1 mm compared to 2 cm in the anodization bath. However, this is compensated by the fact that the electrolyte in the anodization tape is highly viscous and therefore has a much lower specific conductivity. In effect, the experimentally determined electrolyte resistance for bath and tape anodization normalized to the area of the working electrode is very similar (4.0 Ω cm² and 5.0 Ω cm², respectively).

It is well known that the morphology of the anodic oxide is also governed by temperature. A detailed investigation into the temperature effects on anodization using an electrolyte based on sulfuric acid was carried out by Aerts et al. [10]. In the temperature range of 5 - 55 °C, they observed an increase in the porosity of the anodic oxide with increasing temperature, while at the same time its mechanical properties degraded. The authors attributed these effects to a more pronounced chemical dissolution of the oxide at higher temperatures. Interestingly, the pore diameter stayed almost constant between 5 and 35 °C, and only at higher temperatures a strong pore widening occur. In principle, the temperature during anodization can be better controlled in a bath than with a tape geometry. The large volume, and hence heat capacity, of the bath together with the possibility to promote heat transport by stirring effectively limits the temperature increase. However, the experiments carried out in the present work gave no evidence of excessive heating during tape anodization. A maximum temperature

increase of about 5 K was observed, which was not much different from the temperature increase of the bath (approx. 6 K). Obviously, the heat spreading in the aluminum substrate and the heat transport to the sample holder were sufficient to keep the temperature stable during tape anodization.

3.3. TEM investigation

For bath and tape anodization of aluminum AA1050, typical anodic oxide layers with a porous part and a barrier part were obtained. The TEM images for bath and tape anodization for the five measurement points during anodization are shown in Fig. 5.

The TEM lamella prepared by FIB had a thickness of 50 nm to 100 nm. Since the pore diameter in the porous part of the oxide is about 40 nm, the lamella contained several pores in a series. The dark layer on top of the anodic oxide is Pt/Pd, which was deposited on the samples for electrical conductivity.

With increasing anodization and voltage time, the layer thickness of the porous anodic oxide increased (for bath anodization: Fig. 5a - e; for tape anodization: Fig. 5f - j). As the pore diameter linearly depends on the applied voltage [11, 12], a layered structure was observed within the porous part of the anodic oxide. At a P_2 of 12 V (Fig. 5b, g), two sublayers corresponding to 3 V and 12 V were visible. At the beginning of the 25 V hold at P_3 (Fig. 5c, h), the porous layer showed three sublayers with different pore diameters. With ongoing anodization at 25 V, the topmost part of the anodic oxide layer was dissolved at P_4 (Fig. 5d, i). Only for tape anodization were two sublayers within the porous oxide layer still visible at the half time at P_4 (Fig. 5i) and at the end of 25 V hold at P_5 (Fig. 5j). For bath anodization (Fig. 5e), only one layer with a homogenous pore diameter was observed; however, near the surface, the oxide structure is modified by pore thinning. The effect is discussed in greater detail on the basis of the STEM images (see below). This indicates higher dissolution rates for the anodic oxide in bath anodization compared to tape anodization. This effect is probably due to different electrolyte viscosities and, consequently, different rates of mass transport.
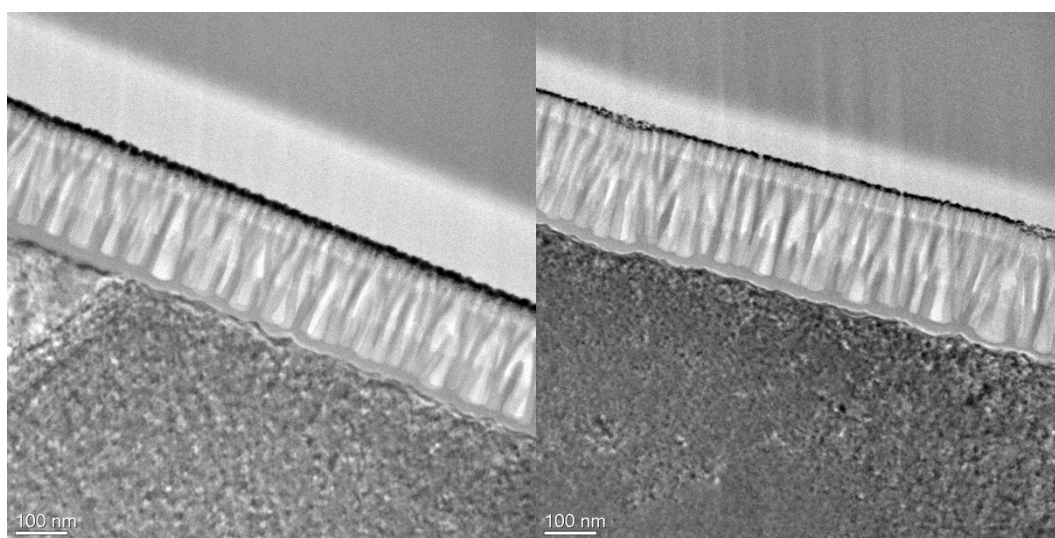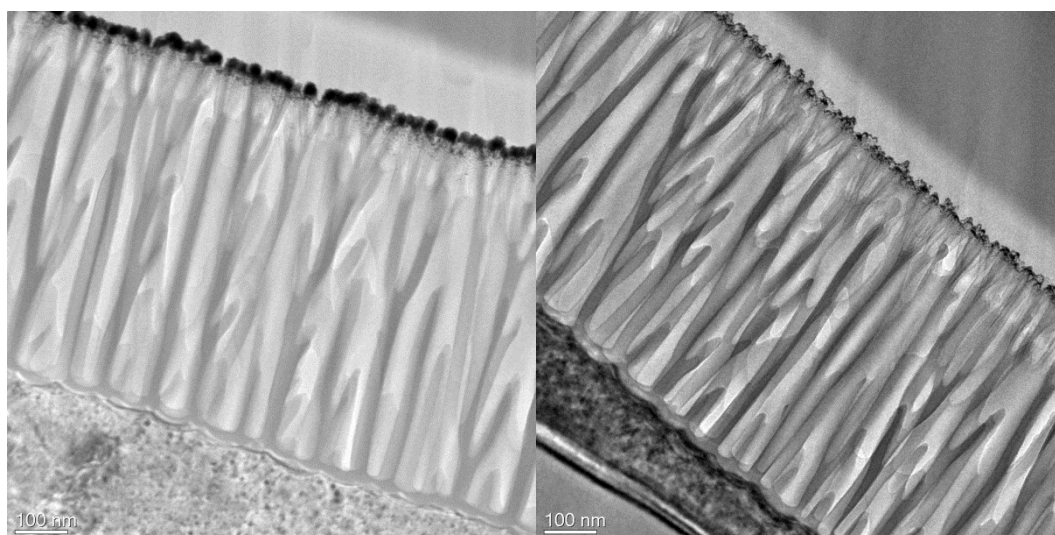

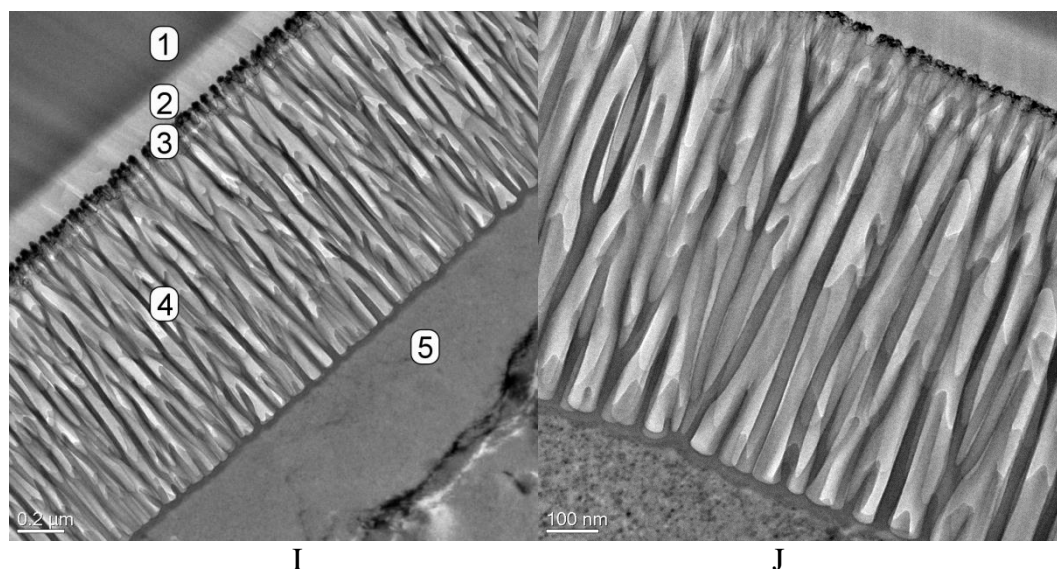A   B

C

D

E

F

G

H

I J
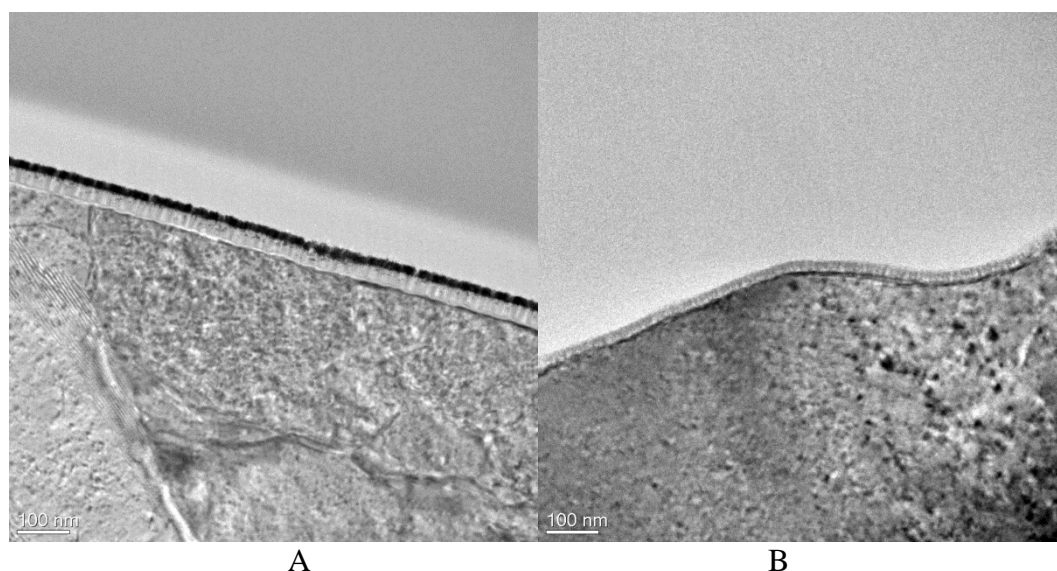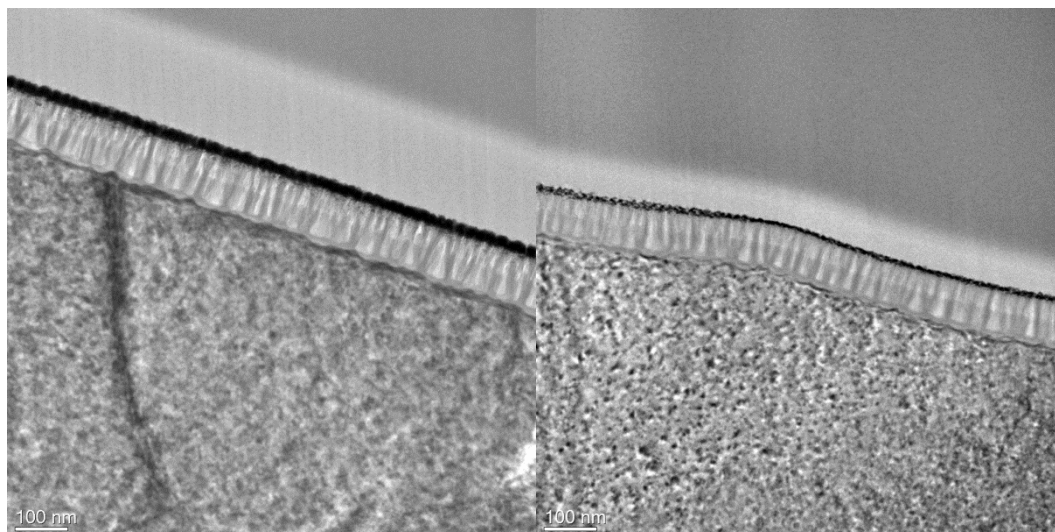
Figure 5. TEM micrographs of anodic oxide layers on AA1050A obtained in bath (a-e) and tape anodization (f-j) at P_1 (3 V) (a+f), at P_2 (12 V) (b+g), at P_3 (the beginning of 25 V-hold) (c+h), at P_4 (the half of 25 V-hold) (d+i) and at P_5 (the end of 25 V-hold) (e+j). With the exception of image i, the image size is 1×1 µm². The sequence of layers is indicated in image i (size 2 x 2 µm²). From top to bottom: ion beam induced deposited carbon (1), electron beam induced deposited carbon (2), layer of platinum and palladium (3), anodic oxide layer (4) and aluminum substrate (5).

In addition to the sublayers formed at different voltage levels, further changes of the oxide morphology were induced by chemical dissolution of the oxide by the electrolyte. Since the top zone of the oxide was the oldest one, and was therefore exposed to the electrolyte for the longest time, a sublayer with partially dissolved pore walls was found at the top of the anodic oxide. This sublayer revealed the same periodicity of pores as contained in the original sublayer that had not yet been attacked by the electrolyte, but with significantly thinned pore walls. These partially dissolved sublayers are found for 10 min of the final voltage hold at P_4 (Fig. 5d, i) and for 20 min at P_5 (Fig. 5e, j) for bath and tape anodization. The partially dissolved sublayers were thicker for bath anodization than for tape anodization. The transition from the sublayer with the original pore structure to the sublayer with pore thinning can be more clearly seen in the scanning transmission electron microscope (STEM) images. As an example, a STEM image of the anodic oxide layers obtained by bath anodization after 20 min at the 25 V hold (P_5) is shown in Fig. 6.

The partially dissolved layer consists of thin filaments that were formed by the continuous chemical dissolution of the pore walls. Nagayama and Tamura have termed this effect the "pore widening mechanism" [13]. Filaments of anodic oxides are formed in electrolytes with high oxide dissolution rates, such as phosphoric acid [14-16]. After longer anodization times, these filaments grow thinner and unstable, and this can finally lead to the formation of a bird nest-type structure on top of the anodic oxide layer. In our case, only the thinning of the pore walls was observed. Any formation of bird nest structures were, if at all, only seen to some extent (topmost 10 nm to 20 nm of the dissolution layer). Instead, a complete dissolution of the oxide is found, which was termed "bulk dissolution" [11].
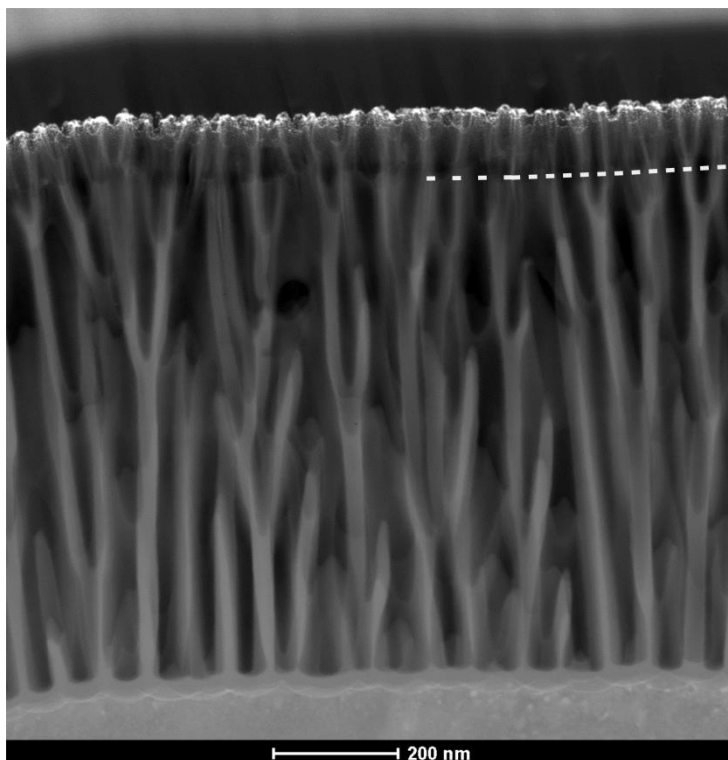
Figure 6. STEM micrograph of anodic oxide layer on AA1050A obtained in bath anodization at P_5. The dashed line indicates the transition from regular porous oxide (bottom) to the dissolution layer (top).

3.4. Total thickness of the anodic oxide layer and thickness of the barrier type oxide layer

The total thicknesses of the porous parts and the thicknesses of the barrier type parts of the anodic oxide layers of tape and bath anodization were evaluated by TEM images of the lamella prepared by FIB (Fig. 7).

For both anodization methods, the total thickness of the anodic oxide layer increased with increasing voltage from 3 V to 25 V (Fig. 7a). For a constant voltage of 25 V, the total oxide layer thickness increased with time. The differences in the total anodic oxide layer thickness between bath and tape anodization were only found for the anodic oxide layer after a longer treatment time during the voltage hold. This is in agreement with the decreasing current density for tape anodization during the voltage hold (Fig. 4). The barrier layer thickness of bath and tape anodization linearly depended on the anodization voltage (Fig. 7b), which is in agreement with previous publications [11, 17]. By evaluating the barrier thickness data from measurement points P_1 to P_3, formation factors of 1.32 ± 0.11 nm V^{-1} were obtained for bath anodization and 1.35 ± 0.09 nm V^{-1} for tape anodization. This is in the range of values published elsewhere, ranging from 0.75 nm V^{-1} to 2 nm V^{-1} [18]. During the voltage hold at 25 V, the barrier layer thickness was nearly constant. The barrier layer thickness was independent of the viscosity and no differences between bath and tape anodization were found [1, 2].
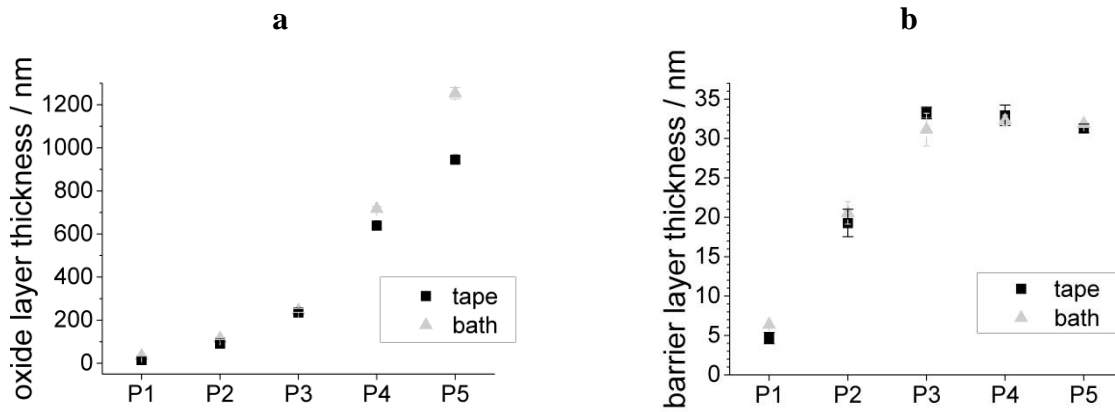
Figure 7. a) Total anodic oxide layer thickness and b) barrier layer thickness during anodization of
tape (black square) and bath anodization (grey triangle) [2].

3.5. Investigation of sublayers

Due to the step-wise voltage evolution at the beginning of the experiment and the linear
dependence of pore diameter on anodization voltage [11, 12], sublayers in the porous part of the
anodic oxide were formed that can be evaluated by TEM images of the lamella prepared by FIB (see
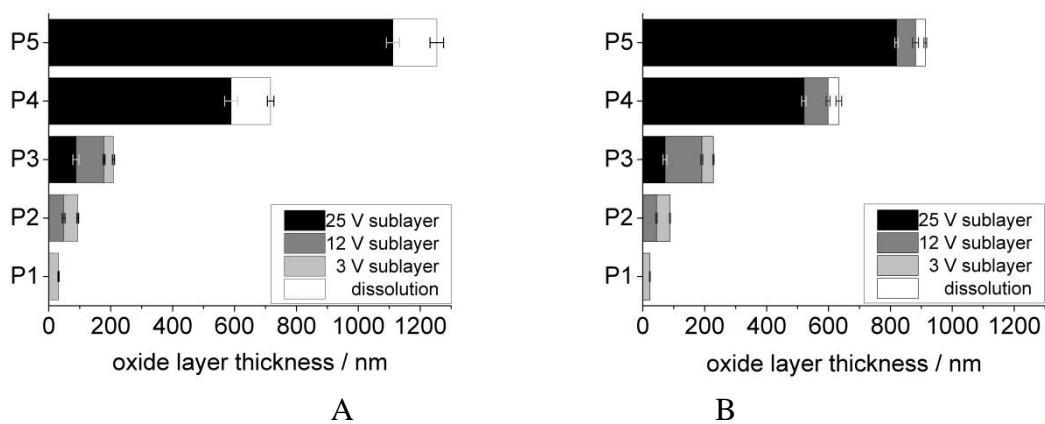Fig. 5). The thicknesses of the sublayers during bath and tape anodization are shown in Fig. 8.

Figure 8. Sublayer thickness of anodic oxide layer during anodization for a) bath and b) tape
anodization at P_1 (3 V), P_2 (12 V), P_3 (beginning of the 25 V hold), P_4 (half of the 25 V hold)
and P_5 (end of the 25 V hold). "Dissolution" indicates a sublayer with partially dissolved pore
walls.

From P_1 with 3 V to the first sample at 25 V (P_3), no clear differences in the sublayers between
bath and tape anodization could be determined. For a longer treatment time, the outer anodic oxide
layers were dissolved by chemical dissolution and the partially dissolved sublayers were observed for
bath and tape anodization. The partially dissolved sublayers for bath anodization were thicker than for
tape anodization and were constant during the voltage hold for both anodization types. The continuous

dissolution of anodic oxide leads to a partially dissolved sublayer with a front that moves from the outside to the inside of the anodic oxide. Oxide dissolution with a complete removal of pore walls in phosphoric acid without pore widening has been investigated by O'Sullivan and Wood and was referred to as "bulk dissolution" [11].

3.6. Oxide formation and dissolution rates of bath and tape anodization

The estimation of oxide formation rates and oxide dissolution rates is complicated due to the simultaneity of the processes [19]. The effective growth rate $r_{growth,effective}$ describes the effective increase in oxide layer thickness during anodization and consists of the oxide formation rate $r_{formation}$ and the oxide dissolution rate $r_{dissolution}$. While the oxide formation rate can only be calculated for sublayers that are covered by previously formed sublayers, the effective growth rate and oxide dissolution rate can only be calculated from outer sublayers without a covering sublayer. Covered sublayers are protected against oxide dissolution, and therefore the oxide formation rate $r_{formation}(P_n, U)$ determined at a given measurement point P_n and formed at the voltage U (values without asterisks in Table 7) can be calculated directly from the sublayer thickness and time the sample was taken according to:

$$r_{formation}(P_n, U) = \frac{d(P_n, U) - d(P_{n-1}, U)}{t(P_n, U) - t(P_{n-1}, U)} \tag{1}$$

where $d(P_n, U)$ is the thickness of the sublayer formed at voltage U determined at measurement point P_n (Table 5 and Table 6) and $t(P_n, U)$ is the duration of the experiment at voltage U up to the measurement point P_n (Table 4). The effective growth rates $r_{growth,effective}(P_n, U)$ are calculated according to Eq. (1) if the outermost sublayer is considered.

Table 5. Sublayer thickness at the different measurement points for bath anodization

$d(P_n, U)$ / nm		P_1	P_2	P_3	P_4	P_5
	3	31 ± 2	46 ± 3	30 ± 3	-	-
U / V	12	-	48 ± 4	91 ± 3	-	-
	25	-	-	88 ± 10	589 ± 21	1112 ± 21
Dissolution layer		-	-	-	85 ± 10	107 ± 22

Table 6. Sublayer thickness at the different measurement points for tape anodization

$d(P_n, U)$ / nm		P_1	P_2	P_3	P_4	P_5
	3	23 ± 1	44 ± 1	38 ± 2	-	-
U / V	12	-	44 ± 2	104 ± 3	78 ± 7	61 ± 10
	25	-	-	72 ± 6	520 ± 7	819 ± 5
Dissolution layer		-	-	-	35 ± 9	32 ± 4

From the changes in sublayers thicknesses and the associated times, the oxide formation rates can be calculated (Table 7).

Table 7. Oxide formation rates of sublayers and the oxide formation rate based on the transported charge according to Eq. (3) for bath and tape anodization in nm s^{-1} for measurement points P_1-P_5

Sublayer	Measurement point	Bath anodization / nm s^{-1}	Tape anodization / nm s^{-1}	Oxide formation rate based on transported charge	
				Bath anodization / nm / (mC cm^{-2})	Tape anodization / nm / (mC cm^{-2})
3 V sublayer	P_1	$\geq 0.37*$	$\geq 0.26*$	≥ 0.49	≥ 0.25
12 V sublayer	P_2	0.56	0.52	0.56	0.43
25 V sublayer	P_3	0.93	0.75	0.72	0.49
	P_4	$\geq 0.87*$	0.78	≥ 0.64	0.55
	P_5	$\geq 0.93*$	0.53	≥ 0.48	0.32

*) Rates marked with asterisks were effective growth rates or minimal oxide formation rates and rates without asterisks were oxide formation rates according to Eq. (1).

For the 12 V and 25 V sublayers of bath and tape anodization at measurement points P_2 and P_3, respectively, the oxide formation rate can be calculated using Eq. (1). More oxide formation rates for the 25 V sublayer can only be calculated for tape anodization, as it is still covered by the 12 V sublayer even with a longer treatment time (P_4 and P_5).

For the outermost 3 V sublayer for both bath and tape anodization, the oxide formation rate between the first measurement point P_1 and the second measurement point P_2 consists of oxide formation and dissolution. Therefore, only an effective growth rate due to the simultaneous oxide dissolution can be calculated for this sublayer according to Eq. (1) with the 3 V sublayer thickness taken from the TEM images.

For bath anodization at 25 V with a longer treatment time, the 25 V sublayer was only covered with the dissolution layer and, consequently, it was dissolved and formed at the same time as the 3 V sublayer previously described. Therefore, at measurement points P_4 and P_5 only a lower limit of the oxide formation rate can be calculated using Eq. (1) for the 25 V sublayer.

Oxide dissolution rates describe the chemical dissolution that leads to a reduction in the thickness of the porous part of the anodic oxide. These rates can be calculated for the measurement points P_n from the oxide formation rate and effective growth rate (Table 7) according to:

$$r_{dissolution}(P_n) = r_{formation}(P_n, U) - r_{growth,effective}(P_n, U) \qquad (2)$$

These rates can only be calculated from the TEM images if no covering sublayer protects the sublayer of interest and only one sublayer is dissolved between the two points of investigation. Therefore, the calculation of oxide dissolution rates is possible for the 3 V sublayer of bath and tape

anodization at measurement point P_3 and only for tape anodization for 12 V at P_5 (values without asterisks in Table 8) according to Eq. (2).

Table 8. Oxide dissolution rates of sublayers for bath and tape anodization in nm s^{-1} for 3 V and 12 V sublayers at P_3 (12 V, 1.5 min), P_4 (25 V, 10.5 min) and P_5 (25 V, 20 min). Rates marked with asterisks are minimal oxide dissolution rates and rates without asterisks were oxide dissolution rates.

Measurement point	Sublayer	Bath anodization [nm s^{-1}]	Tape anodization [nm s^{-1}]
P_3	3 V sublayer	0.10	0.04
P_4	12 V + 3 V sublayer	$\geq 0.21^*$	-
P_5	12 V sublayer	-	0.02

For P_4 of bath anodization, the calculation of the lower limit of the dissolution rate is based on the assumption that only the 12 V sublayer and the 3 V sublayer are dissolved between measurement points P_3 and P_4. If part of the 25 V sublayer is dissolved as well, the oxide dissolution rate can be higher than the estimated 0.21 nm s^{-1}.

The oxide formation rates of the sublayers formed at different voltages given in Table 7 clearly increase with increasing voltage for both types of anodization. This is expected because at higher current densities more Al^{3+} ions are formed at the aluminum surface, leading to a higher oxide formation rate. For bath anodization, the oxide formation rate increases from 0.37 nm s^{-1} to 0.93 nm s^{-1} during increasing voltage from 3 V to 25 V. A similar increase between 3 V (0.26 nm s^{-1}) and 25 V (0.75 nm s^{-1}) can be detected for tape anodization.

For an overall growth of a porous anodic oxide during constant voltage, the oxide formation rate must be higher than the oxide dissolution rate [12]. This is valid for all sublayers of tape and bath anodization. For example, at P_5 we find an effective growth rate of 0.7 nm s^{-1} at a current density of 1.5 mA cm^{-2} for bath anodization and 0.5 nm s^{-1} at 1.0 mA cm^{-2} for tape anodization (by use of Eq. 2). The differences in the effective growth rate between bath and tape are obviously related to current density. Effective growth rates normalized to current density are 0.48 nm s^{-1}/mA cm^{-2} (bath anodization) and 0.51 nm s^{-1}/mA cm^{-2} (tape anodization), and therefore they are very similar.

Camprestini et al. published an effective growth rate for PAA of 2.1 nm s^{-1}. The investigation was performed in 0.4 M phosphoric acid at 5 mA cm^{-2} (under galvanostatic control) [20], corresponding to 0.42 nm s^{-1}/mA cm^{-2}. Diggle et al. investigated the increase in the porous oxide layer thickness during anodization in 10% sulfuric acid at 10 mA cm^{-2}. The effective growth rate that can be estimated from a plot of the porous oxide layer thickness against anodization time [17] is 4.2 nm s^{-1} (normalized 0.42 nm s^{-1}/mA cm^{-2}). Taking into account the differences in experimental conditions (electrolyte, current density), it can be concluded that our data are in good agreement with those published by the cited authors.

For $t < 10$ min (P_1, P_2 and P_3), the oxide formation rates only reveal a small influence of the electrolyte viscosity for the 3 V and 25 V sublayers. For both sublayers, the oxide formation rate of

bath anodization is slightly higher than the pertinent oxide formation rate of the tape anodization. For t > 10 min (P_4 and P_5), only a lower limit of the oxide formation rate or growth rate for bath anodization can be calculated. It is clearly higher than the oxide formation rate for tape anodization. While oxide formation rates of bath anodization during the voltage hold at 25 V (P_3 - P_4) were constant with time, or even increased slightly, the oxide formation rate for the tape anodization decreased with time. These trends of the oxide formation rate are in good agreement with the current density response of bath and tape anodization (Fig. 4). The current density of tape anodization decreased with time, the reaction rate of oxide formation slowed down, and consequently the oxide formation rates led to smaller oxide layer thickness in comparison with bath anodization (Fig. 7a).

In order to evaluate the relationship between current density during anodization and the oxide formation rate, the corresponding oxide formation rates based on transferred charge during anodization were calculated by sublayer thickness and transported charge during anodization (Eq. 3). The obtained values are also listed in Table 7.

$$r_{formation,Q}(P_{n-1}, U) = \frac{d(P_n,U) - d(P_{n-1},U)}{Q(P_n,U) - Q(P_{n-1},U)} \tag{3}$$

The transferred charge for every sublayer at the measurement points can be determined from the integral of current density over the time according to:

$$Q(Pn, U) = \int_{t_{n-1}}^{t_n} j(t)dt \tag{4}$$

where j is the current density and t the time. All results are listed in Table 7.

For bath anodization, the oxide dissolution rate increased with higher anodization voltage. Between P_3 and P_4, the oxide dissolution rate is at least twice as high because only a lower limit of the oxide dissolution rate for the 12 V sublayer of bath anodization can be determined. For tape anodization, no significant difference can be deduced. These results are in agreement with investigations into the oxide dissolution rates of bath and tape anodization without any voltage applied. For that purpose, the specimens were anodized first by normal bath or tape anodization at 25 V for 20 min. After anodization, the samples were exposed without any applied voltage to the electrolyte (PAA or anodization tape) for 40 min. The chemical dissolution rates without applied voltage determined by this experiment are listed in Table 9.

Table 9. Oxide dissolution rates of bath and tape anodization in nm s^{-1} for currentless exposure of 40 min after normal anodization (25 V, 20 min, 6 V min^{-1}).

	Bath anodization	Tape anodization
Oxide dissolution rate without current flow [nm s^{-1}]	0.14	0.006

Similar results were published in a previous paper for a currentless exposure time of 15 min [1]. For a currentless exposure time of 15 min and 40 min, a chemical dissolution with a decrease in oxide layer thickness was found for bath anodization. For tape anodization, the oxide layer thickness was almost unchanged after 40 min. Only the pore walls were thinned according to the pore widening mechanism described by Nagayama and Tamura [13]. The trend of different dissolution rates for bath

and tape anodization that was found for currentless exposure is confirmed by the present investigation during anodization. Typically, dissolution rates are higher during anodization and increase with increasing anodization voltage.

Oh et al. found a dependence of the oxide dissolution rate during anodization on the applied electric field [19]. They developed a discontinuous anodization process for the investigation of oxide dissolution without simultaneous oxide formation. Therefore, in the first step a barrier oxide layer was formed and in the second step of the discontinuous anodization process the oxide layer was anodized in an aggressively dissolving electrolyte of 5 wt.% phosphoric acid. For chemical dissolution without an electric field, they found an oxide dissolution rate of 0.004 nm s^{-1}. At a voltage of 86 V, the initial dissolution rate is similar to that without an electric field, but increases to 0.0075 nm s^{-1} after 20 min. In consideration of the different content of phosphoric acid and the applied voltage, the oxide dissolution rates during anodization are in the range of published values.

Ono and Masuko estimated oxide dissolution rates by a pore-filling technique [21]. They found an influence of incorporated phosphate anions on the oxide dissolution rate. For barrier layers of porous anodic oxide films, three layers with different amounts of phosphate were identified by determination of different oxide dissolution rates. From the electrolyte/oxide interface with bulk aluminum, the incorporation of phosphate ions decreased. The dissolution rate of the outer anodic oxide layers formed in 0.4 mol dm^{-3} phosphoric acid at 20 V (0.0017 nm s^{-1}) was clearly different from that of the inner oxide layer (0.0005 nm s^{-1}) [21]. These values for dissolution rates are lower compared to the dissolution rates for bath and tape anodization in our investigation. Because Ono and Masuko used 2 mol dm^{-3} sulfuric acid for the investigation of oxide dissolution instead of phosphoric acid, lower dissolution rates can be expected.

For a direct comparison of oxide dissolution rates between bath and tape anodization, valid data are only available for the 3 V sublayer. An additional comparison for the estimation of the difference between bath and tape anodization is possible for sublayers formed at 12 V. Therefore, the estimated minimal oxide dissolution rate of bath anodization can be compared to the oxide dissolution rate of tape anodization. For both cases, the oxide dissolution rate is clearly higher for bath anodization. The same difference can be derived from the experiment with a currentless exposure time of 40 min. Investigations with and without voltage show that the oxide dissolution rate of tape anodization is almost negligible. A higher thickness of the dissolution layer for bath anodization with an average value of 95 nm, in comparison to 33 nm of tape anodization, also shows higher oxide dissolution in PAA. This can be explained by the different chemical properties of the anodic oxides or by a limited mass transport in the tape electrolyte, which leads to local bath aging [17]. The high viscosity of tape anodization leads to a reduced mass transport and can therefore result in lower oxide dissolutions rates.

Schneider et al. investigated the effect of bath aging by the anodization of aluminum in phosphoric acid [17]. As a consequence of anodization, the concentration of aluminum cations in the anodization electrolyte increases due to the chemical and electric field assisted dissolution and the direct injection. The increase of aluminum cations leads to a substitution of protons in the electrolyte and consequently to an increase in specific electrical resistance. A decrease of protons by chemical dissolution results in an increase of the pH value and in lower oxide dissolution rates. Schneider et al. found this effect for electrolyte baths that were used for more than 10 h [17]. For tape anodization, it is

possible that a local aging of the electrolyte at the substrate surface caused by reduced mass transport enhances the effect on lower oxide dissolution rates due to high viscosity.

Another consequence of reduced mass transport in case of tape anodization can be a partial blocking of the anodized surface by the products of the anodization process. According cryo-TEM investigations conducted in our previous work [2], these residues form a fuzzy cloud-like layer located directly on top of the anodic oxide. As could be shown by in-situ EIS measurements the degree of coverage continuously increases during the final stage of anodization at 25 V ($P_3 - P_5$). Although the exact chemical composition of these residues is not known yet, the available EDX data suggest that the cloud-like layer consists of an organic gel possibly stabilized by aluminum ions. It is highly likely that the reduction of current density starting at P_3 can be attributed to the formation of a blocking layer. Reduction of current density is also the main reason why the oxide formation rates for tape anodization are significantly lower than for bath anodization. However, it should be noted that tape anodization is generally less efficient than bath anodization. This becomes obvious when growth rates with respect to transferred charge are compared (Table 7). Growth rates normalized to charge Q for the anodization tape are generally lower by 20% – 95% than for the bath. This effect is clearly not related to partial blocking of the anodic oxide, because it is already detectable at the early stages of tape anodization where no cloud-like blocking layer is present.

The dissolution rates of anodic oxide are very low for tape anodization. As the dissolution rates further decrease with ongoing anodization, it is reasonable to assume that the cloud-like layer also has a protective effect on the underlying oxide, slowing down the chemical attack by the acidic electrolyte.

4. CONCLUSIONS

Oxide formation and oxide dissolution rates for conventional bath anodization and a novel tape anodization process were determined by TEM investigations. The structure of the sublayers formed by abrupt voltage changes during anodization process allowed a determination of the rates without additional experiment and lead to a better understanding of the influence of the high electrolyte viscosity of the novel anodization tape.

- Oxide formation rates for bath anodization (PAA) and for tape anodization increase with increasing voltage, which corresponds to an increasing current density. The oxide formation rate is higher for bath than for tape anodization due to reduced mass transport because of the extremely high viscosity of the anodization tape. During the voltage hold at 25 V, the oxide formation rate continuously decreases for tape anodization and is nearly constant for bath anodization. These trends correspond to current density responses and show a reduction of mass transport for a longer treatment time in the high viscous electrolyte of the tape anodization.

- Oxide formation rates normalized to current density show similar results for both kind of anodization. The normalization on current density allows a comparison with experimental results in the literature, where other electrolytes and condition were used, and shows a good agreement.

- Oxide dissolution increases with voltage for bath anodization and, therefore, chemical dissolution depends on the applied electric field. For tape anodization, the oxide dissolution is nearly

negligible because only pore widening and the formation of a partially dissolved layer can be observed.

- The lower oxide formation rates for tape anodization are partly compensated by the very small dissolution rates. In effect, the final thickness of the porous oxide formed by the anodization tape was only by 25% smaller than for a conventional bath process.

References

1. L. Berndt, A. Hartwig, M. Kleemeier, A. Krieger, K. Thiel and M. Burchardt, *Surf. Interface Anal.*, 48 (2016) 926.
2. L. Berndt, M. Kleemeier, K. Thiel, A. Hartwig and M. Burchardt, Formation of anodic oxide layers in highly viscous phosphoric acid PART 1: Investigation by scanning electron microscopy (SEM) and in-situ electrochemical impedance spectroscopy (in-situ EIS), Int. J. Electrochem. Sci. (2018) in print.
3. J.C. Norris, *Plat. Surf. Finish.*, 78 (1991) 36.
4. J.C. Norris, *Galvano-Organo-Trait Surf*, 64 (1995) 141.
5. http://www.dalicworld.com/dalicstick_gb.html.
6. C.L. Ong, W.Y. Shu and S.B. Shen, *Int. J. Adhes. Adhes.*, 12 (1992) 79.
7. L. Bergan, *Int. J. Adhes. Adhes.*, 19 (1999) 199.
8. ASTM D 3933 - 98 Standard Guide for Preparation of Aluminum Surfaces for Structural Adhesives Bonding (Phosphoric Acid Anodizing), ASTM International.
9. P.G. Sheasby, R. Pinner and S. Wernick, The surface treatment and finishing of aluminium and its alloys, 6th ed., Finishing Publication Ltd., UK, 2001.
10. T. Aerts, Th. Dimogerontakis, I. De Graeve, J. Fransaer and H. Terryn, *Surf. Coat. Tech.* 201 (2007) 7310
11. J.P. O'Sullivan and G.C. Wood, *Proc. R. Soc. London, Ser. A*, 317 (1970) 511.
12. M. v.Put, Potentiodynamic anodizing and adhesive bonding of aluminium for the aerospace industry, Department of Materials Science and Engineering, Delft University of Technology, Delft, 2013.
13. M. Nagayama and K. Tamura, *Electrochim. Acta*, 12 (1967) 1097.
14. J. Ye, Q. Yin and Y. Zhou, *Thin Solid Films*, 517 (2009) 6012.
15. M. Schneider, K. Kremmer, S. Weidmann and W. Fürbeth, *Surf. Interface Anal.*, 45 (2013) 1503.
16. M. Schneider and K. Kremmer, *Surf. Coat. Tech.*, 246 (2014) 64.
17. J.W. Diggle, T.C. Downie and C. Goulding, *Chem. Rev.*, 69 (1969) 365.
18. M. Lohrengel, *Mater. Sci. Eng., R*, 11 (1993) 243.
19. J. Oh and C.V. Thompson, *Electrochim. Acta*, 56 (2011) 4044.
20. P. Campestrini, G.E. Thompson, P. Skeldon, C.E. Blanco-Pinzon, L. Iglesias-Rubianes and S.J. Garcia-Vergara, *Proc. R. Soc. Ser. A*, 462 (2006) 2345.
21. S. Ono and N. Masuko, *Journal of Japan Institute of Light Metals*, 43 (1993) 447.